Mechanism of the $^{26}Mg(^{18}O,^{16}O)^{28}Mg$ reaction at $E_{^{18}O} = 50$ MeV and the energy levels of ^{28}Mg

M. Bernas, M. Roy-Stephan, F. Pougheon, M. Langevin, G. Rotbard, and P. Roussel
Institut de Physique Nucléaire, 91406 Orsay, France

J. P. LeFèvre, M. C. Lemaire, and K. S. Low
Département de Physique Nucléaire, CEN Saclay, BP No. 2, 91190 Gif-sur-Yvette, France

B. H. Wildenthal
Institut de Physique Nucléaire, 91406 Orsay, France
and Cyclotron Laboratory, Michigan State University, East Lansing, Michigan 48824
(Received 10 July 1978; revised manuscript received 6 February 1979)

The reaction $^{26}Mg(^{18}O,^{16}O)^{28}Mg$ has been studied at a bombarding energy of 50 MeV between laboratory angles of 4° and 17°. The differential cross sections of the lowest four states of ^{28}Mg have been compared to exact finite-range calculations in the distorted-wave Born approximation and coupled-channels Born approximation formulations. The reaction-mechanism calculations employed wave functions for the initial and final nuclear states which were generated in shell-model calculations carried out in the full $d_{5/2}$-$s_{1/2}$-$d_{3/2}$ basis space. The relative importance of one-step and two-step processes in the population of the different final states is evaluated and the effectiveness of current reaction theories in accounting for phenomena such as are exemplified by the present data is discussed.

[NUCLEAR REACTIONS $^{26}Mg(^{18}O,^{16}O)^{28}Mg$; enriched target, $E=50$ MeV, measured $\sigma(\theta)$, microscopic DWBA and CCBA analysis with shell-model wave functions; deduced levels of ^{28}Mg.]

I. INTRODUCTION

We have studied the $^{26}Mg(^{18}O, ^{16}O)\,^{28}Mg$ reaction with the aim of obtaining additional information about the level structure of ^{28}Mg, about which relatively little is known,[1-3] and of further elucidating the mechanism of heavy-ion two-nucleon transfer reactions, in particular the role of coupling between the inelastic-scattering and two-nucleon-transfer processes. In this report we present the results of analyzing the transitions to the lowest few states of ^{28}Mg with distorted-wave Born-approximation (DWBA) and coupled-channels Born-approximation (CCBA) calculations based on shell-model wave functions, together with results for the excitation energies and differential cross sections of the high-lying excited states which are strongly populated in this reaction.

The competition between the single-step transfer of a two-nucleon cluster from the target ground state to a given residual level and two-step processes connecting these same two levels which involve inelastic excitation of an intermediate state in either the target or residual nucleus (either before or after the transfer of the two-nucleon cluster) has been found to be significant in a variety of contexts. Studies have been carried out with targets in the light,[4,5] medium[6-9] and heavy regions[10,11] and with both light-ion and heavy-ion beams. When heavy-ion beams are utilized, the inelastic excitation of the projectile, such as ^{18}O in the present case, can also play a role.[7,8,12] The present study is the first to combine a heavy-ion initiated reaction with the sort of detailed shell-model wave functions typically available only for lighter ($A \leq 40$) nuclei.

The study of the stripping of two neutrons onto ^{26}Mg to form states of ^{28}Mg offers a particularly clear avenue into the delineation of the relative importance of single-step and multiple-step reaction processes. This arises from the quasiclosure of the $d_{5/2}$ neutron orbit in the ^{26}Mg ground state, the wave function of which has as its leading term (relative to the ^{16}O core) $[d^{\nu}_{5/2}]^{6}_{J=0}\,[d^{\pi}_{5/2}]^{4}_{J=0}$. The ground state of ^{28}Mg, which can similarly be approximated as $[d^{\nu}_{5/2}]^{6}_{J=0}\,[s^{\nu}_{1/2}]^{2}_{J=0}\,[d^{\pi}_{5/2}]^{4}_{J=0}$, can be directly populated by the addition of two neutrons in the $s_{1/2}$ orbit coupled to $J=0$. (More realistically, of course, the spread of the wave function over the adjacent shell-model orbits means that the actual transfer involves $J=0$ pairs of neutrons in each of the $d_{5/2}$, $s_{1/2}$, and $d_{3/2}$ orbits, insofar as the explicit theoretical wave functions utilized here are concerned, and even beyond that in nature. The simple point to be made is just that the "ground state to ground state" transition is "allowed.")

The dominant term of the wave function of the lowest 2^+ level of ^{28}Mg should be $[d^{\nu}_{5/2}]^{6}_{J=0}\,[s^{\nu}_{1/2}]^{2}_{J=0}$

$[d^{\pi}_{5/2}]^{4}_{J=2}$. (The value of $J=2$ must come from the protons of this configuration because of the full $d_{5/2}$ neutron orbit and inability to construct $J=2$ from $j=\frac{1}{2}$.) Alternate neutron configurations involving the $d_{3/2}$ orbit lie appreciably higher in unperturbed energy. This term, with its protons coupled to $J=2$, cannot be reached by a single-step direct transfer of two neutrons from the ground state of ^{26}Mg, in which the protons are coupled to $J=0$. Thus, on a qualitative level, it can be inferred that direct population of the first excited state of ^{28}Mg via two-neutron stripping should be suppressed relative to population of the ^{28}Mg ground state. When explicit wave functions for the states concerned are considered, it will be found that this effect does emerge quite strongly, as the lowest 2^+ appears to be dominated by proton excitations. This juxtaposition of "forbidden" and "allowed" transitions in the study of coupled-channels effects is analogous to the approach taken by Yagi *et al.*[13] in the study of (^{12}C, ^{14}C) leading to the $N=82$ closed-shell nucleus ^{142}Nd.

Our principal attention here is focused on these two levels, the 0^+ ground state and 2^+ first excited state of ^{28}Mg. The shell-model calculation from which we have taken the wave functions used to describe ^{26}Mg and ^{28}Mg appear to account best for the properties of the lowest few levels in a given system. This, when combined with the qualitative "allowed" vs "forbidden" natures of the ground state and first excited state transitions, leads us to hope that the analyses we make of these transitions will not contain major uncertainties in the description of the nuclear structure of the states involved. Our goal here is to study the reaction mechanism with minimal ambiguity from the nuclear structure assumptions.

II. EXPERIMENTAL PROCEDURE

The $^{26}Mg(^{18}O, ^{16}O)^{28}Mg$ reaction was initiated with a 50 MeV beam of ^{18}O from the Orsay MP tandem Van de Graaff accelerator. The targets were enriched (99.7%) ^{26}Mg, 100 ± 10 $\mu g\,cm^{-2}$ thick, supported on layers of 25 $\mu g\,cm^{-2}$ of carbon and 1 $\mu g\,cm^{-2}$ gold and covered with a 7 $\mu g\,cm^{-2}$ layer of carbon. The particles emergent from the target were momentum analyzed in an $n=\frac{1}{2}$ magnetic spectrograph. The acceptance solid angle was 2.25×10^{-4} sr, with an angular width of ±7 mrad, so that the oscillatory structure of the angular distributions could be easily resolved.

The particles were detected in the kinematically corrected focal plane of the spectrograph by a

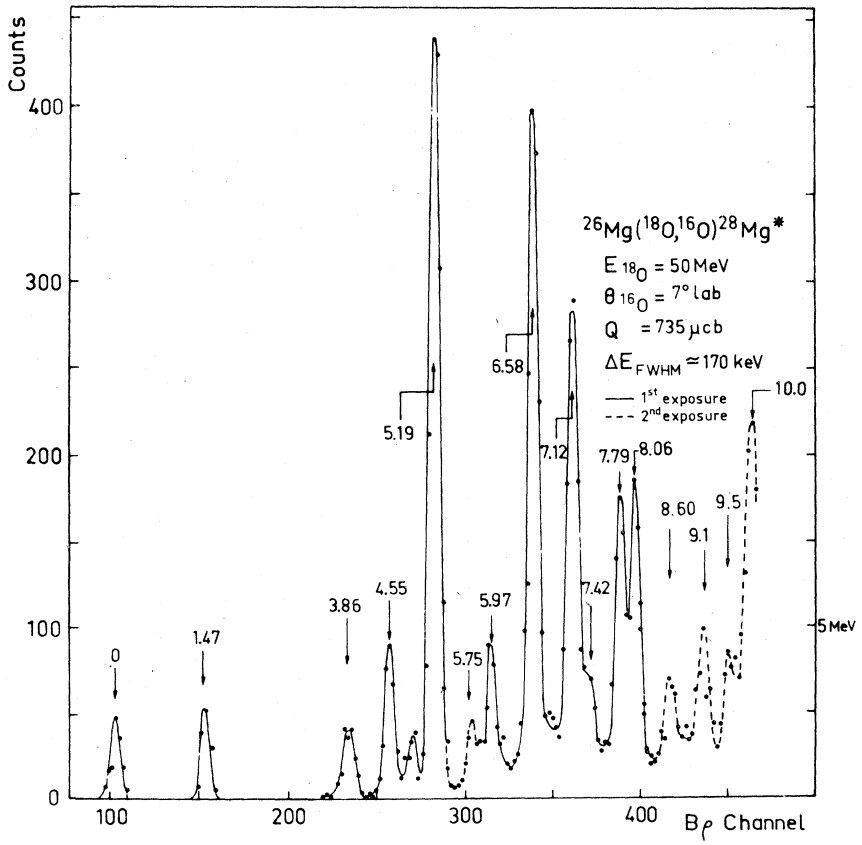

Fig. 1. $^{26}Mg(^{18}O, ^{16}O)^{28}Mg$ spectrum at $\theta_{lab} = 7°$.

combination of a (transmission) single-wire, current-dividing counter,[14] which measured the energy loss ΔE of the particles and their position along the focal plane, and two (stopping) 100×10 mm^2 silicon detectors, which measured the residual energy (E-ΔE) of the particles. The typical resolution for (^{18}O, ^{16}O) in the present measurements ranged between 140 and 210 keV. A typical spectrum is shown in Fig. 1.

A surface-barrier detector located at $\theta_{lab} = 40°$ in the scattering chamber was used to monitor elastic scattering from the target. This monitor counting served to internormalize the intensities of the spectra measured at different angles. The deadtime corrections for the spectra were made by feeding the ADC deadtime back to the beam current integrator electronics. Corrections were typically 4% and always less than 10%. The spectrograph magnetic field was chosen so that the ^{16}O spectra collected correspond to the 8^+ charge state, the most probable state for these energies. Corrections for the other charge states were made according to Ref. 15. The total uncertainty in the differential cross section (resulting from a combination of charge-state averaging, deadtime corrections, solid-angle ratios, geometrical efficiency, etc.) is estimated to be 25%.

The overall cross section scale for the present data was assigned relative to the differential cross sections for the elastic (^{18}O, ^{18}O) scattering measured at the most forward angles. These differential cross sections were assumed to have the values calculated from the optical-model code MAGALI.[28] These elastic-scattering data are presented in Fig. 2.

The calibration for the ^{28}Mg energy level spectra is based upon the previously known[1] energies of the ground, 1.47, 3.86, and 4.55 MeV states. The uncertainties in the assigned energies for the states in the 6–10 MeV region of excitation are 60 keV.

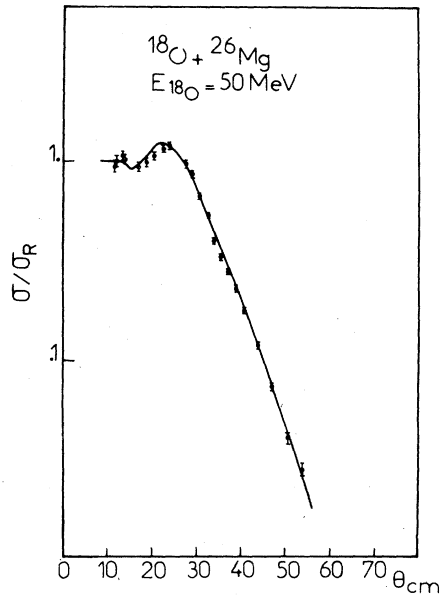

FIG. 2. Elastic-scattering angular distribution measured between 12° and 54° c.m. fitted with the entrance channel sets of parameters $P1, P2, P3$.

III. EXPERIMENTAL RESULTS

A. Strongly excited states

Of the previously known levels of ^{28}Mg, the lowest four (0^+_1, 2^+_1, 0^+_2, and 2^+_2) and the $1^- - 3^-$ doublet at 5.19 MeV are significantly populated in the present reaction. A comparison of the (^{18}O, ^{16}O) cross sections to those of the corresponding (t, p) reaction[1] is made in Fig. 3. We see that relative to the ground state the 2^+_1, 0^+_2, 2^+_2, and $1^- - 3^-$ are more strongly populated in (^{18}O, ^{16}O) by factors of roughly 2 to 3, but that the same qualitative profile exists in both reactions. Momentum matching conditions in the present (^{18}O, ^{16}O) reaction should enhance L transfers of 2, 3, and 4 in the vicinity of 4.7 MeV excitation.[16,17] Lack of (t, p) data above 6 MeV makes it impossible to check whether the strongly populated levels seen here at 6.58, 7.12, 7.79, and 8.06 MeV also dominate the spectrum in this light-ion transfer case. Inspection of a spectrum from a recent ^{26}Mg(^{4}He, ^{2}He)^{28}Mg experiment[18] shows three strongly populated states, at excitation energies of 6.46, 8.88, and 9.78 MeV. These states presumably have high spin values (5^-, 6^+). The two levels populated in (^{18}O, ^{16}O), which are closest in energy to these three, are those observed in (^{18}O, ^{16}O) at 6.58 and 10 MeV. The selectivity shown in the present data is very similar to that observed in our preliminary observations of (^{18}O, ^{16}O) at 90 MeV.

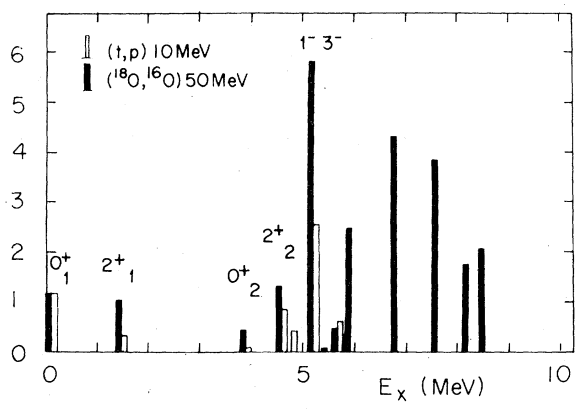

FIG. 3. Comparison for the states of ^{28}Mg between intensities integrated from 5° to 25° c.m. for the 10 MeV (t, p) reaction (1) and for the 50 MeV (^{18}O, ^{16}O) reaction.

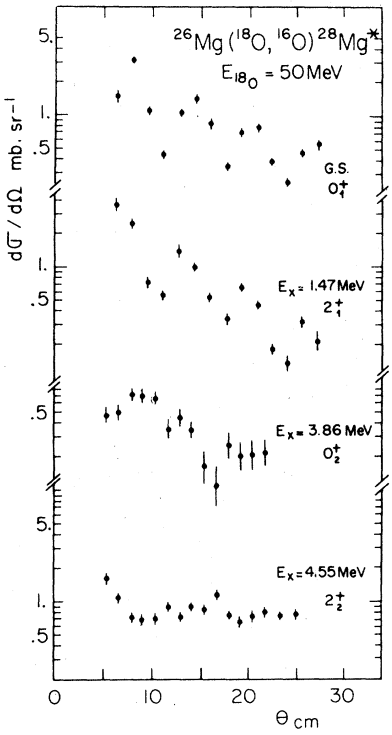

FIG. 4. Angular distributions of $^{26}Mg(^{18}O, ^{16}O)\ ^{28}Mg$ for the four first levels of ^{28}Mg.

B. Angular distributions

Differential cross sections were measured for $5° \leq \theta_{c.m.} \leq 25°$ for levels of ^{28}Mg below 9 MeV excitation. The angular distributions for the lowest four levels are shown in Fig. 4. The ground and first excited state distributions are strongly oscillatory, while this feature is progressively attenuated for the third and fourth states. The experimental measurements were extended as far forward in angle as feasible in an attempt to obtain relatively model-independent characteristics of different L transfer.[19,20] The two 2^+ states show increasing strength from 11° to 5° while the 0^+ states have distributions which peak at 9°.

The angular distributions for the strongly populated states (or groups of states) above 5 MeV excitation are presented in Fig. 5. They all exhibit very little angular structure. This rather uniform lack of distinctiveness makes it impossible to use the observed shapes to further spectroscopic assignments in this region. On the basis of strength alone we can infer that these levels have natural spin-parity and probable spins $2 \leq J \leq 5$. In combination with definite spin-parity assignments from further studies, the currently observed intensities should be useful in delineating the configurations of these levels.

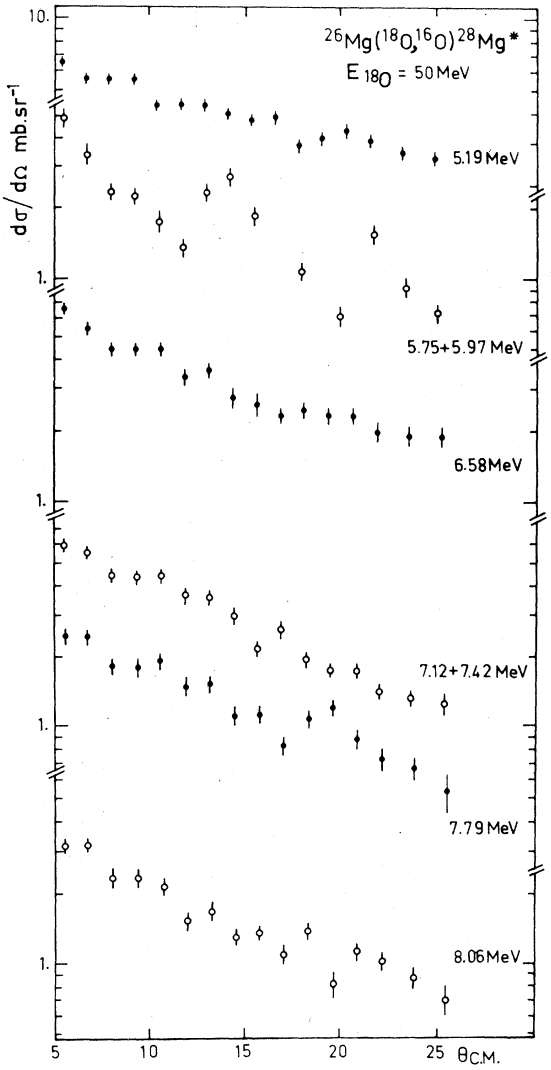

FIG. 5. Angular distributions of $^{26}Mg(^{18}O,^{16}O)^{28}Mg$ for the ^{28}Mg levels with greater than 5 MeV excitation energy.

IV. ANALYSIS OF $^{26}Mg(^{18}O,^{16}O)^{28}Mg$ DIFFERENTIAL CROSS SECTIONS WITH EFR-DWBA AND EFR-CCBA CALCULATIONS

We have analyzed the data of the two-neutron transfers to the low-lying states of ^{28}Mg alternatively in the framework of the DWBA and CCBA, utilizing the codes SATURN-MARS I and II, written by Tamura, Low, and Udagawa.[21] A review[22] of the formulation of the EFR-DWBA and EFR-CCBA transfer amplitudes shows that the EFR-CCBA matrix element can be written schematically as

$$T_{\text{EFR-CCBA}} = \sum_{\substack{A',a' \\ B',b'}} \iint \chi^{(-)*}_{b'B'}(\vec{k}_{b'},\vec{r}_{b'})\langle I_{B'}M_{B'}\, S_{b'}M_{b'}|V|I_{A'}\, M_{A'}S_{a'}M_{a'}\rangle \chi^{(+)}_{A'a'}(\vec{k}_{a'},\vec{r}_{a'})\, d\vec{r}_a d\vec{r}_b\,. \tag{1}$$

The wave functions $\chi^{(+)}$ and $\chi^{(-)}$ are the generalized distorted waves of the entrance and exit channels, respectively, which account for elastic- and inelastic-scattering cross sections simultaneously. The brackets $\langle \| \rangle$ represent the form factors describing the transition matrix elements between the various entrance and exit channel states incorporated into the calculation. The summation over A', B', a', and b' takes account of the various routes by which a given residual state can be reached from the target state; examples of such routes for only the ground and first excited states of ^{26}Mg and ^{28}Mg are shown in Fig. 6.

In the above formulation, the DWBA corresponds to the limit of vanishing inelastic excitations in the entrance and exit channels. For the example of Fig. 6, for instance, all routes which involve inelastic excitations would be dropped from consideration and the summation reduced to a single term. In this formulation of the model, the $\chi^{(+)}$ and $\chi^{(-)}$ scattering wave functions would account only for the elastic-scattering channels in the context of the ordinary optical model.

In Sec. IV A we describe the detailed formulation of the form factors which are used in both the DWBA and CCBA calculations. In Sec. IV B we present and discuss the results of the DWBA calculations and in Sec. IV C the results of the CCBA calculations.

A. The two-nucleon form factor

In both DWBA and CCBA calculations the form factors have the form

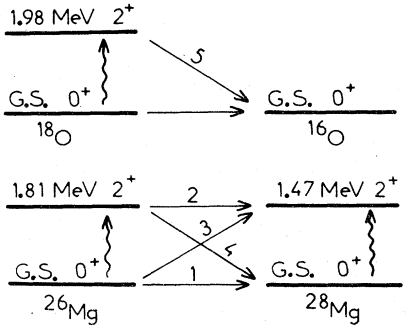

FIG. 6. Diagram of the different transition routes taken into account in the CCBA calculations. In this case the two-step routes proceed via target and residual nucleus inelastic excitation and via projectile excitation.

$$\langle I_B M_B S_b M_b|V|I_A M_A S_a M_a\rangle = \int \langle I_B M_B|I_A M_A\rangle \langle S_b M_b|V|S_a M_a\rangle\, d\epsilon_x\,, \tag{2}$$

where $d\epsilon_x$ denotes the internal coordinates of the transferred nucleons. In the present calculations, the transferred nucleons are assumed to form a cluster. Therefore, the integration over x is merely a sum over the spin and isospin variables as in the case of a single-nucleon transfer. In the post representation of the (^{18}O, ^{16}O) reaction, the potential $V = V_{bx}(R_2)$ represents the interaction which binds the neutron pair (described as a cluster) to the ^{16}O core.

The overlap functions on the right-hand side of Eq. (2) are expressed in terms of the two-nucleon spectroscopic amplitudes B and antisymmetrized two-nucleon wave functions Φ,

$$\langle I_B M_B|I_A M_A\rangle = \sum_{\mu\mu' j} B^{(BA)}_{(\mu\mu' j)} \langle I_A M_A\, jm_j|I_B M_B\rangle \times \Phi_{jm_j\mu\mu'}(\vec{r}_1,\vec{r}_1') \tag{3}$$

and

$$\langle S_a M_a|V|S_b M_b\rangle = \sum_{\nu\nu' s} B^{(ba)}_{(\nu\nu' s)} \langle S_a M_a\, sm_s|S_b M_b\rangle \times \Phi_{sm_s\nu\nu'}(\vec{r}_2,\vec{r}_2')\,.$$

Here the brackets represent the usual Clebsh-Gordan coefficients and the indices $\mu(\mu',\nu,\nu')$ stand for the quantum numbers $n_\mu l_\mu j_\mu$ of each transferred nucleon. The quantum numbers jm_j (sm_s) are the total spin and spin projection of the pair of nucleons in the residual nucleus B (in the projectile a).

By use of the transformation from j-j to L-S coupling and the Talmi-Moshinsky transformation, the two-nucleon wave functions can be expressed in a form in which the motion of the center of mass of the two-nucleon system, represented by $\Phi_{NL}(R)$, can be separated from the relative motion of the two nucleons, represented by $\phi_{n_x l_x}(r)$:

$$\Phi_{jm_j\mu\mu'}=[2(1+\delta_{\mu\mu'})]^{-1/2}\sum\begin{vmatrix} l_\mu & \frac{1}{2} & j_\mu \\ l_{\mu'} & \frac{1}{2} & j_{\mu'} \\ \lambda & s_x & j \end{vmatrix}[1-(-1)^{s_x+l_x+t_x}]\langle n_\mu l_\mu n_{\mu'} l_{\mu'},\lambda | n_x l_x N L\lambda\rangle\{[\phi_{n_x l_x}(\vec{r})\Phi_{NL}(\vec{R})]_\lambda \chi_{s_x}(\sigma_1\sigma_2)\}_j , \tag{4}$$

where the [ ] are the usual jj to L-S transformation coefficients and $\langle|\rangle$ are the coefficients of the Talmi-Moshinsky transformation tabulated by Brody and Moshinsky.[23] In this transformation, the angular momentum λ has to satisfy the following selection rules:

$$\vec{\lambda}=\vec{l}_\mu+\vec{l}_{\mu'}=\vec{l}_x+\vec{L}\,.$$

The indices s_x and t_x are the spin and isospin of the transferred pair.

By utilizing these expansions the form factors can now be written down in a fashion similar to that employed for the case of one-nucleon-transfer reactions [Eq. (2-12) of Ref. 21],

$$F_{lsj}=\sum_{N_1L_1N_2L_2} d^{lsj}_{N_1L_1N_2L_2}[\Phi_{N_1L_1}(\vec{R}_1)V_{bx}(\vec{R}_2)\Phi_{N_2L_2}(\vec{R}_2)]_{lm_l} \times \hat{S}_a\hat{I}_B g^{lsj}_{AaBb}\,, \tag{5}$$

where S_a and I_B are the spins of the projectile and residual nuclei, $\hat{S}_a$ stands for $(2S_a+1)^{1/2}$, g^{lsj}_{AaBb} corresponds to Clebsch-Gordan coefficients and phase factors (Ref. 21). The quantities s and j are the spins of the transferred pair respectively in the projectile and residual nucleus and l is the angular momentum transferred. They satisfy the following selection rules:

$$\vec{j}=\vec{l}+\vec{s}\,,$$
$$\vec{j}=\vec{I}_B-\vec{I}_A\,,$$
$$\vec{s}=\vec{S}_b-\vec{S}_a\,,$$

where I_A, I_B, S_a, and S_b are the spins of the target, residual nucleus, projectile, and ejectile.

The spectroscopic amplitudes d are defined as

$$d^{lsj}_{N_1L_1N_2L_2}=\sum_{\substack{N_1L_1n_xl_x \\ N_2L_2n'_xl'_x}} C^{(1)}_{I_BI_Aj}\,C^{(2)}_{S_aS_bs}(-1)^{s_x+L_2-s} \times W(L_1L_2js,ls_x)\Omega_{n'_xn_xl_x}\,, \tag{6}$$

where

$$C^{(1)}_{I_BI_Aj}=\sum_{\mu\mu'\lambda_1} B^{(BA)}_{\mu\mu'j}\begin{bmatrix} l_\mu & \frac{1}{2} & j_\mu \\ l_{\mu'} & \frac{1}{2} & j_{\mu'} \\ \lambda & s_x & j \end{bmatrix}\langle n_\mu l_\mu n_{\mu'} l_{\mu'}|n_x l_x N_1 L_1\lambda_1\rangle\hat{\lambda}_1\hat{I}_x W(L_1l_xjs_x;\lambda_1,I_x)(-1)^{l_x+L_1-\lambda_1}\frac{1}{(1+\delta_{\mu\mu'})^{1/2}}\,. \tag{7}$$

The analogous expression for $C^{(2)}_{S_aS_bs}$ follows the form of Eq. (7). The term $\Omega_{n_xn'_xl_x}$ describes the overlap between the wave functions of the relative motion of the two nucleons. We assume in the present calculations that the two neutrons are transferred in a relative $0s$ configuration so that a single value of N describes the center-of-mass motion of the pair.

The center-of-mass wave functions $\Phi_{NL}(R)$ were generated in a Woods-Saxon potential which had a radius $R=1.25\,A_c^{1/3}$ fm, where A_c is the mass of the core, and a diffuseness of $a=0.65$ fm. The two-nucleon amplitudes $B(\mu\mu' j)$ which connect the different states of ^{26}Mg and ^{28}Mg were calculated from the complete $d_{5/2}$-$s_{1/2}$-$d_{3/2}$ space shell-model wave functions of Chung and Wildenthal.[24] These B values are listed in Table I and the corresponding $d^{lsj}_{N_1L_1N_2L_2}$ values are given in Table II. Also given in Table II are the d values corresponding to pure two-particle configurations appropriate to the various initial and final states.

From Table II quantitative estimates of the suppression of the first excited-state transition relative to the ground-state transition can be obtained. The DWBA cross sections are proportional to the squares of the d factors. Thus it can be seen that the realistic wave functions

TABLE I. Two-nucleon spectroscopic amplitudes calculated from shell-model wave functions of Ref. 24. The signs of these spectroscopic amplitudes are given with Condon-Shortley phase convention and assuming the radial part of the wave function to be positive at the origin.

		$(d_{5/2})^2$	$(d_{5/2}, s_{1/2})$	$(d_{5/2}, d_{3/2})$	$(s_{1/2})^2$	$(s_{1/2}, d_{3/2})$	$(d_{3/2})^2$
$^{26}Mg \rightarrow {}^{28}Mg$							
$0_1^+ \rightarrow 0_1^+$		0.5139			0.5399		0.4504
$0_1^+ \rightarrow 2_1^+$		−0.0049	0.0559	0.0037		−0.2906	−0.1578
$2_1^+ \rightarrow 0_1^+$		−0.2415	−0.5559	−0.0829		+0.1433	+0.0978
$2_1^+ \rightarrow 2_1^+$	$\Delta J=0$	−0.4930			−0.3843		−0.4196
	$\Delta J=1$			−0.0490		−0.0288	
	$\Delta J=2$	0.0172	0.1308	0.0560		−0.1467	−0.1307
	$\Delta J=3$		−0.0371	−0.0660			
	$\Delta J=4$	−0.0350		0.3013			
$0_1^+ \rightarrow 0_2^+$		0.0258			−0.4402		0.3762
$0_1^+ \rightarrow 2_2^+$		−0.0701	−0.1031	0.0399		−0.3536	−0.0859
$^{18}O \rightarrow {}^{16}O$							
$0_1^+ \rightarrow 0_1^+$		−0.866			−0.413		−0.283
$2_1^+ \rightarrow 0_1^+$		−0.821	−0.506	−0.061		−0.220	−0.131

TABLE II. Reduced spectroscopic amplitudes for the $^{26}Mg(^{18}O, ^{16}O)^{28}Mg$ reaction. The signs of these spectroscopic amplitudes are given with time reversal phase convention and assuming the radial part of the wave function to be positive at infinity.

^{18}O	^{16}O	^{26}Mg	^{28}Mg	N_1	L_1	N_2	L_2	$dN_1L_1N_2L_2$	Pure configuration
0_1^+	0_1^+	0_1^+	0_1^+	2	0	2	0	+0.2801	$+0.1437(s_{1/2})^2$
		0_1^+	2_1^+	2	0	1	2	−0.0418	$+0.0340(s_{1/2}, d_{3/2})$
		2_1^+	0_1^+	2	0	1	2	−0.0914	$-0.0215(d_{3/2})^2$
		2_1^+	2_1^+	2	0	2	0	+0.2345	
2_1^+	0_1^+	0_1^+	0_1^+	1	2	2	0	−0.460	
0_1^+	0_1^+	0_1^+	0_2^+	2	0	2	0	+0.051	
		0_1^+	2_2^+	2	0	1	2	+0.033	

TABLE III. Optical model parameters used in the DWBA (sets $P1, P2, P3$) and the CCBA (sets $CC1$, $CC2, CC3$) calculations.

		V	r_{ov}	a_v	W	r_{ow}	a_w	r_{oc}
$P1$	^{18}O	40.19	1.374	0.548	66.86	1.374	0.326	1.374
	^{16}O	22.27	1.374	0.530	6.98	1.370	0.360	1.370
$P2$	^{18}O	37.65	1.453	0.428	78.0	1.412	0.230	1.453
	^{16}O	37.0	1.350	0.404	78.0	1.290	0.174	1.350
$P3$	^{18}O	26.98	1.35	0.618	51.59	1.23	0.552	1.35
	^{16}O	100	1.35	0.618	23.40	1.23	0.552	1.35
$CC1$	^{18}O	37.47	1.374	0.548	17.10	1.374	0.784	1.17
	^{16}O	37.47	1.374	0.548	17.10	1.374	0.784	1.17
$CC2$	^{18}O	37.47	1.374	0.548	17.10	1.374	0.784	1.17
	^{16}O	23.65	1.31	0.490	5.25	1.311	0.300	1.17
$CC3$	^{18}O	33.63	1.374	0.548	48.13	1.374	0.326	1.17
	^{16}O	33.63	1.374	0.548	48.13	1.374	0.326	1.17

yield an enhancement of a factor of 4 over the already allowed transfer of a pure $(1s_{1/2})^2_{J=0,T=1}$ pair while the cross section of the first excited state is suppressed by a factor of 4 from that of a pure $(1s_{1/2}0d_{3/2})_{J=2,T=1}$ transfer.

B. The EFR-DWBA calculations

1. The optical-model parameters

The various sets of optical-model-parameter values which were used in the DWBA calculations are listed in Table III. Parameters for the exit channel, $^{16}O+^{28}Mg$, have been chosen to be consistent with the results of various analyses of the elastic scattering of ^{16}O on nuclei neighboring ^{28}Mg at energies comparable to that employed in the present study. The parameter sets $P1$ and $P2$ have geometries determined from analyses of $^{16}O+^{24}Mg$ elastic scattering[25,26] while the parameter set $P3$ has the geometry of the potential determined from a simultaneous analysis of $^{16}O+^{28}Si$ elastic scattering at several different energies.[27] The parameters for the entrance channel, $^{18}O+^{26}Mg$, have been determined from an optical-model analysis (utilizing the code MAGALI[28]) of the elastic-scattering data measured in the present experiment. Since our measurements cover only a limited angular range and hence are far from sufficient to fix all of the optical-model parameters unambiguously, we have chosen to impose an approximate consistency between entrance and exit channel geometries by initiating the parameter searches to fit our data at different starting values corresponding to the geometries of sets $P1$, $P2$, and $P3$ for the exit channel.

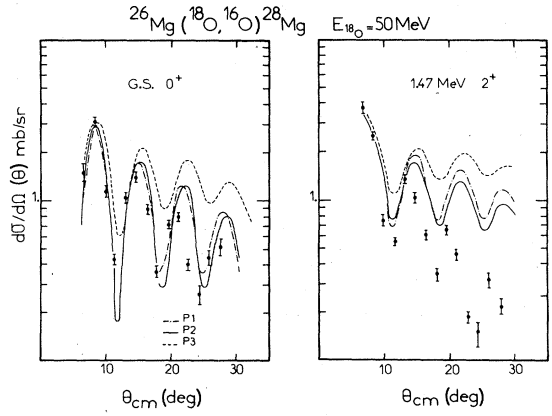

FIG. 7. DWBA fits with the different sets of parameters $P1$, $P2$, and $P3$ (Table III) for the 0^+_1 and 2^+_1 levels of ^{28}Mg populated with the $^{26}Mg(^{18}O,^{16}O)^{28}Mg$ reaction.

2. Shapes of angular distributions

The angular distributions for the transfer cross sections to the ground and first excited states of ^{28}Mg which are calculated in the DWBA with these three sets of optical-model parameters are shown in Fig. 7, in comparison to the experimental data. The calculations for the $J=0^+$ ground state with sets $P1$ and $P2$ succeed fairly well in describing the angular periodicity and the amplitude of the oscillations, and the rate with which the envelope of intensity of the angular distribution decreases in magnitude with increasing angle. The angular distribution calculated with parameter set $P3$ fails to display either the experimentally observed amplitude of oscillation or decreasing envelope of intensity.

The three corresponding angular distributions calculated for the $J=2^+$ first excited state have the same relationship to each other as do the ground-state distributions. The calculations with sets $P1$ and $P2$ are very similar while that with set $P3$ displays smaller amplitude of oscillation and a slower decrease of intensity envelope with increasing angle. The agreement between the calculated and experimentally observed angular distributions is considerably poorer than that obtained for the ground state, however, particularly in that the envelope of intensity of the measured distribution decreases with angle much more rapidly than do those of the calculated distributions. Calculations with several parameter sets other than those of Table III have been carried out in an attempt to achieve

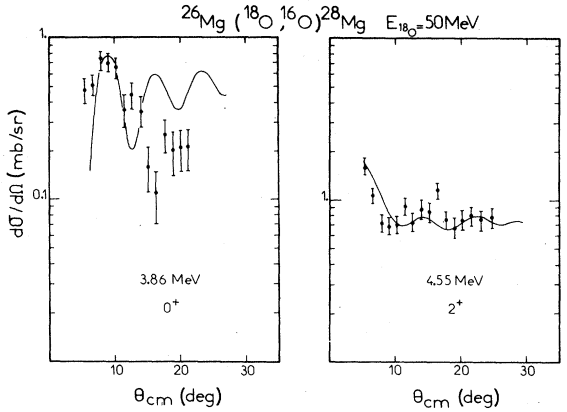

FIG. 8. Angular distributions of the $^{26}Mg(^{18}O,^{16}O)^{28}Mg$ reaction leading to the 3.86 MeV, 0^+_2 and 4.55 MeV, 2^+_2 states. The theoretical angular distributions have been obtained in the framework of an EFR-DWBA calculation using the optical-model parameter set of $P1$ of Table III. The normalization factors between the EFR-DWBA and the experimental cross sections are listed in Table IV.

better agreement with the observed distribution of the first excited state, but without success.

Calculations with parameter set $P1$ yield angular distributions for the 0^+ state at 3.86 MeV and the 2^+ state of 4.55 MeV which are shown in comparison to the measured data in Fig. 8. The calculated shape for the 0_2^+ state does not resemble the observed angular distribution. On the other hand, the calculated and measured shapes for the 2_2^+ state are in reasonable agreement.

The inference which can possibly be drawn from this comparison of DWBA shapes and measured angular distributions is that the DWBA (the assumption of a direct single-step cluster transfer) suffices to account for the 0_1^+ and 2_2^+ transitions but is inadequate to account for the 2_1^+ and 0_2^+ transitions.[29]

3. *Normalization factors for* EFR-DWBA *calculations*

At the present stage of DWBA and CCBA calculations it still seems profitable to separately consider questions of angular distribution shapes (just discussed for the DWBA calculations) and the overall normalizations of the intensities of various transitions. The area of intensity normalization can further be factored into questions of "absolute" and "relative" normalization. We refer to calculated cross section values via the "normalization factors N" of Table IV. The numbers are the ratios of the experimental to the calculated scales when the first oscillation of the calculated curves are superimposed upon the data points as shown in the figures.

It can be seen from Table IV that the values of N are quite sensitive to the choice of optical-model parameters. This sensitivity, together with uncertainties about what the "correct" absolute normalization should be in calculations of the present type, prompts us to concentrate exclusively in this study upon values of N of one final state relative to another. Inspection of Table IV shows that these relative values, indicated by $R = N(J_\nu^\pi)/N(0_1^+)$, are quite insensitive to optical-model parameter variations and are hence meaningful criteria for judging the underlying validity of the reaction theory even though knowledge of the appropriate optical-model parameters might be lacking.

Relative to the ground-state normalization the predicted intensities for the 2_1^+ and 0_2^+ states are much too small. We immediately remember that it was just these two states for which the calculated angular distribution shapes were in bad agreement with experiment. Considering shape and overall magnitude together, it appears that these states are predominantly populated by some other mechanism than that incorporated into the DWBA. In contrast, the 2_2^+ state, whose shape was reasonably well fitted by the DWBA curve, is predicted to be more strongly populated than the 2_1^+ by a factor of 5 (3 from structure, 1.7 from Q dependence in DWBA) and the N value for it is consistent with that of the ground state.

Insofar as the absolute normalization factors are concerned, it appears that the calculated cross sections are too small whatever optical potential parameter set we use. Such discrepancies between the calculated and experimental cross sections have already been found in previous studies of the (^{18}O, ^{16}O) reaction.[30,31] The effects of using more realistic form factors and the importance of sequential one-nucleon-transfer processes have been investigated by Feng *et al.*[32] They found that with the inclusion of these effects the absolute magnitude of the cross section was predicted within a factor of 2 in a great number of two-nucleon-transfer reactions. The increase in the calculated cross section came partly from the

TABLE IV. Absolute (N) and relative (R) normalization factors for the DWBA and CCBA calculations.

		EFR-DWBA			EFR-CCBA		
E_{exc} (MeV)	J^π	OP [a]	N	R	OP [b]	N	R
0.0	0_1^+	$P1$	9.57	1	$CC1$	33	1
		$P2$	7.65	1	$CC2$	60.5	1
		$P3$	11.48	1	$CC3$	15	1
1.47	2_1^+	$P1$	211	22	$CC1$	133	4
		$P2$	157	20	$CC2$	434	7.2
		$P3$	229	20	$CC3$	12	0.8
3.86	0_2^+	$P1$	120	12.5			
4.55	2_2^+	$P1$	29	3			

[a] Optical-model parameters of Table III used in the EFR-DWBA calculation.

[b] Optical-model parameters of Table III used in the EFR-CCBA calculations with target, residual, and projectile inelastic excitation.

microscopic form factor used in the one-step process but to a larger extent came from the significant strength predicted for the sequential transfer. While these additional components in a reaction mechanism must ultimately be included in an analysis of data such as discussed here, the complete synthesis is beyond the scope of our present work.

C. The EFR-CCBA calculations

1. The generalized optical-model parameters

The two-step reaction can proceed by the excitation of the Mg 2_1^+ excited states and of the ^{18}O 2_1^+ excited state as was already pointed out in several analyses of (^{18}O, ^{16}O) and (^{16}O, ^{18}O) reactions.[7,8]

The set of generalized entrance-channel parameters needed as input to the CCBA calculations has been determined by combining the information on the elastic scattering of ^{18}O on ^{26}Mg with those of the B(E2) values for the 2_1^+ excited states of ^{18}O and ^{26}Mg. The elastic-scattering angular distribution was reanalyzed in a coupled-channel framework with the code ECIS.[33]

For ^{26}Mg the $0_1^+ - 2_1^+$ B(E2) value used[34] is 350 $e^2\,fm^4$ which gives, with $\beta_N R_N = \beta_C R_C = 1.62$ fm; a value of β_2 equal to 0.398 with a prolate deformation. For ^{18}O, the deformation parameter currently used, $\beta_2 = 0.367$, has been derived from the experimental data.[35]

The different optical-model parameter sets appear in Table III: The first set *CC*1 refers to a fit of the elastic-scattering data with the ECIS code, starting from the values of set P1 in which both radius $r_V = r_W$ and real diffuseness a_V were held fixed, other parameters being free. The exit channel parameters were arbitrarily taken to be the same as the entrance channel ones, as they are not accessible to direct measurements.

For the second set, *CC*2, the entrance channel parameters are the same as in *CC*1 but the exit channel parameters have been taken from the Siemssen analysis[36] and are compatible with the inelastic scattering to the 2_1^+ of ^{24}Mg.[37] In this case, an oblate deformation was taken for ^{28}Mg with the $B(E2)$ value for the $2^+ \rightarrow 0^+$ transition of 73.9 $e^2\,fm^4$ (Ref. 38); then $\beta_2 R_0^2$ is 6.71 fm^2, which gives a β_2 value of -0.398.

The *CC*3 parameters set results from the optimization of the entrance channel calculation with the geometries held fixed to the values of set *P*1 while only the depths of the real and imaginary potential were varied. Both depths were reduced by 25% from this analysis. The exit channels parameters were taken to be the same as the entrance channel ones.

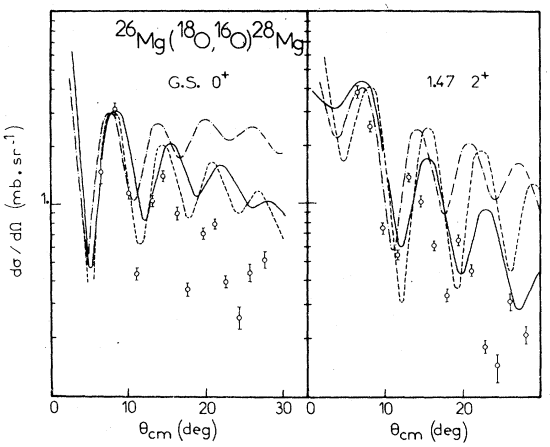

FIG. 9. Angular distributions of the $^{26}Mg(^{18}O,^{16}O)$ reaction leading to the ^{28}Mg ground-state and 2^+ first excited states. The solid lines have been obtained with EFR-CCBA calculations including the transitions displayed in Fig. 6 and using the optical-model parameter sets of Table III with the following convention: The dot-dashed curves correspond to optical parameters set *CC*1, the dashed curves correspond to optical parameters set *CC*2, and the solid curve corresponds to optical parameters set *CC*3. The normalization factors are listed in Table IV.

2. Shapes of angular distributions from EFR-CCBA *calculations*

The angular distributions calculated for the 0_1^+ and 2_1^+ transitions in EFR-CCBA with the three listed sets of optical-model parameters *CC*1, *CC*2, and *CC*3 are compared with the experimental data in Fig. 9.

The CCBA shapes for the ground state yield fits which are comparable to those obtained with the DWBA calculation. The parameter set *CC*1 provides oscillations which are too shallow and an intensity envelope which decreases too slowly with angle. The oscillatory structure and intensity envelope is improved with the set *CC*2.

The curve representing the results obtained with parameter set *CC*3 yields a similar intensity envelope but the angular periodicity is increased. The results suggest that with the optimum parameter values a reasonably quantitative fit to the data should be forthcoming.

The CCBA curves for the 2_1^+ first excited state are in markedly better agreement with the data than were the DWBA results. The results with the parameters sets *CC*1, *CC*2, and *CC*3 have similar relationships to each other and the data as were just noted in the discussion of the ground state. Again it seems probable that a more ju-

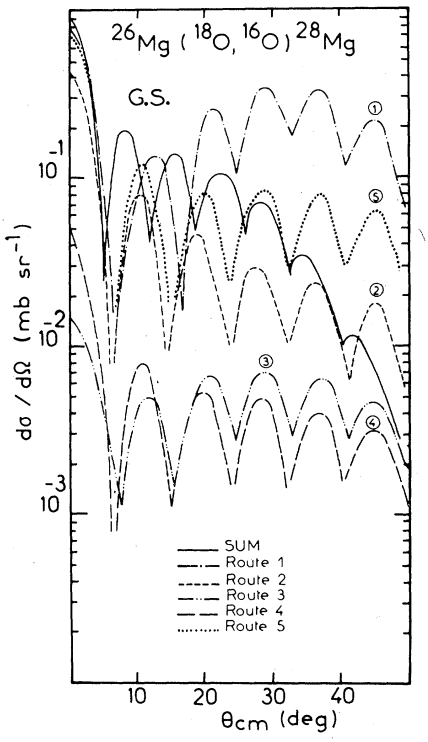

FIG. 10. Relative contributions of the different routes included in the EFR-CCBA calculation of the 0_1^+ state using parameter set *CC*3.

dicious choice of the parameters would provide a quantitative fit to the data.

3. *Normalization factors from* EFR-CCBA *calculations*

As in the case of the DWBA calculations we can concentrate upon the relative normalization factor as the least parameter-dependent aspect of the reaction theory calculations and therefore the more meaningful in the context of the basic validity of the theoretical approach. We use the same concepts and definitions for cross section definitions as for the DWBA results. The results which appear in Table IV may be summarized succintly. The N values for the ground-state transition exhibit sensitivity to the generalized optical-model parameters. The most "successful" parameter set, *CC*3, yields values similar to that obtained with set P3 in DWBA. A dramatic change, however, occurs in the relative normalization for the 2_1^+ transition. These change from about 20 in the DWBA analysis to 0.8 to 7 in the CCBA analysis with the preferred *CC*3 set yielding almost 1. This improvement, which brings the two transitions into relatively good agreement, would seem to validate the underlying corrections of the CCBA approach for understanding the strength of the "forbidden" 2_1^+ transition.

4. *Influence of projectile excitation*

The various routes by which the states of ^{28}Mg can be populated via coupled channels in the ^{26}Mg(^{18}O, ^{16}O)^{28}Mg reaction (see Fig. 6) affect the total differential cross sections in a fashion which depends significantly upon the optical-model parameters. The yields of the various individual routes are shown for 0_1^+ and 2_1^+ in Figs. 10 and 11 for a particular choice of optical-model parameters. The importance of the "projectile excitation" route and its sensitivity to optical parameters are illustrated by Figs. 12 and 13, in which the fully coherent summations of the various routes have been made by alternately including and excluding "projectile excitation." With parameter set *CC*3 this route (route "5") is very important. This would seem to be associated with the less diffuse imaginary potential of set *CC*3.

V. CONCLUSION

Study of the ^{26}Mg(^{18}O, ^{16}O)^{28}Mg reaction to the lowest four states of ^{28}Mg, in particular to the 0_1^+ ground state and the 2_1^+ first excited state, yields the following conclusions: As expected, the 2_1^+ is populated predominantly via non-single-step processes, while the transition to the 0_1^+

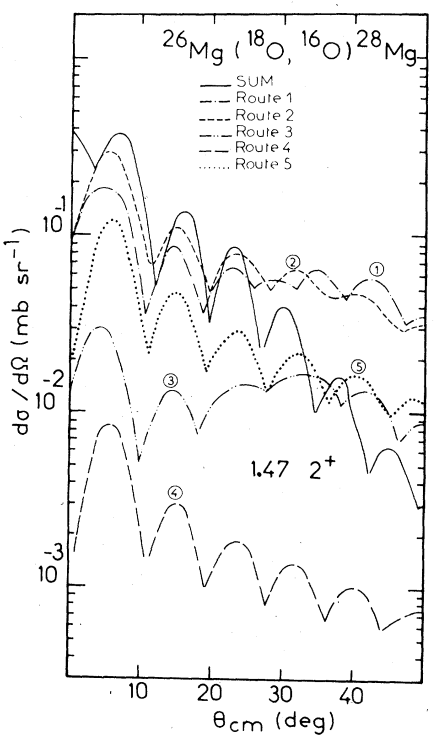

FIG. 11. Relative contributions of the different routes included in the EFR-CCBA calculation of the 2_1^+ state using parameter set *CC*3.

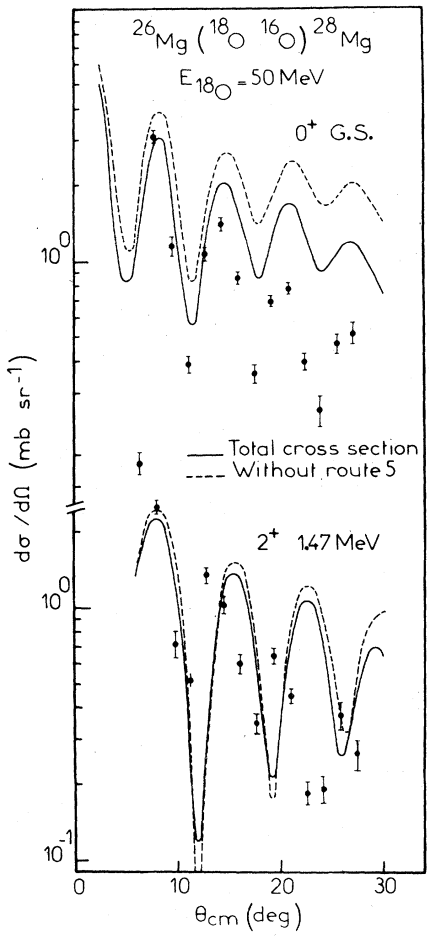

FIG. 12. Contribution of the projectile excitation with parameters set *CC*2 and normalization factors $N(0) = 62.5$ and $N(2) = 244$.

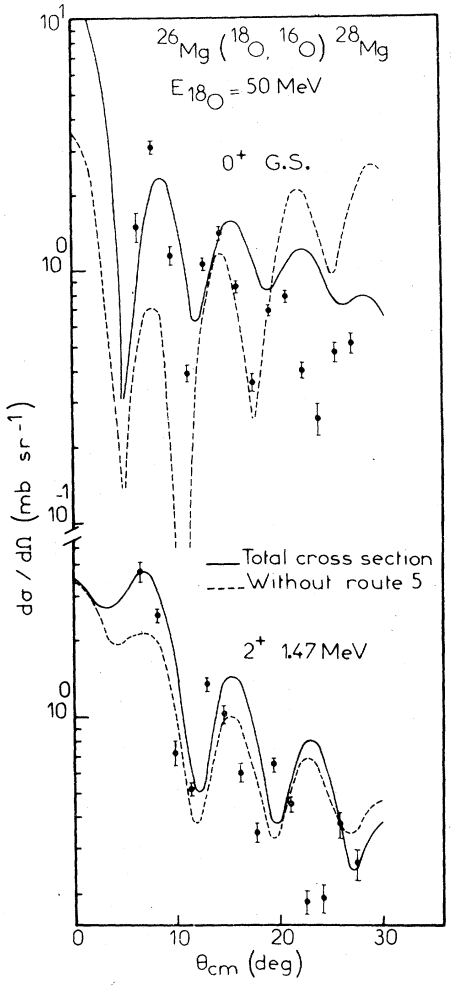

FIG. 13. Contribution of the projectile excitation with parameters set *CC*3 and normalization factors $N(0) = N(2) = 11$.

state proceeds by basically a single-step cluster transfer. This follows from two observations. First, the EFR-DWBA calculations for the 2_1^+ state fail to account for the shape of the measured angular distribution and predict cross sections which are too small by an order of magnitude, while at the same time properly accounting for both the shape and magnitude of the 0_1^+ transition. Second, the expansion of the reaction theory to incorporate competing two-step "inelastic excitation-transfer" paths for the formation of these states accounts for the shape of the 2_1^+ and rectifies the dramatic discrepancy in its relative normalization, while leaving the results for the 0_1^+ transition unimpaired.

It is concluded that EFR-CCBA calculations as currently formulated suffice to yield a qualitatively correct accounting of transitions dominated by multistep processes. The shapes calculated in the EFR-CCBA do not yield exact fits to the data, but the level of knowledge about the appropriate types of parameter families which should be used in CCBA calculations is still rudimentary. The other area from which discrepancies may originate is that of sequential transfer of single nucleons, which was not included in the present treatment. It seems likely that much of the remaining difficulties with the CCBA analysis lie in these areas. Further experimental and analytical work on elastic and inelastic scattering in these mass-energy ranges is certainly needed to help better specify the potential parameters. Also, additional transfer data of the present type is needed to fully delineate the normal and anomalous characteristics of these types of data. This should facilitate a critique of the reaction theory results and may be necessary to a final choice, among the various options, of the correct optical-model characterization.

ACKNOWLEDGMENT

We thank R. Ashari and E. Kashy for their participation in the different stages of the work. We want to acknowledge the hospitality of the CEA staff, in particular B. Berthier and G. Berg for their assistance with the calibration measurement. One of us, B. H. Wildenthal, wishes to acknowledge the support of the U. S. National Science Foundation and the John Simon Guggenheim Memorial Foundation.

[1]R. Middleton and J. Pullen, Nucl. Phys. 51, 77 (1974).
[2]B. Rastegar, G. Guillaume, P. Fintz, and A. Gallman, Nucl. Phys. A225, 80 (1974).
[3]P. Fintz, B. Rastegar, N. E. Davison, F. Hibou, G. Guillaume, and A. Gallman, Nucl. Phys. A197, 423 (1972).
[4]S. Fortier and S. Galès, Phys. Lett. 78B, 52 (1978).
[5]P. Christensen *et al.*, Phys. Lett. 45B, 107 (1973); B. Sorensen, *ibid.* 53B, 285 (1974).
[6]C. F. Maguire, D. L. Hendrie, U. Jahnke, J. Mahoney, D. K. Scott, J. S. Vaagen, R. J. Ascuitto, and K. Kumar, Phys. Rev. Lett. 40, 358 (1978).
[7]P. D. Bond, H. J. Korner, M. C. Lemaire, D. J. Pisano, and C. E. Thorn, Phys. Rev. C 16, 177 (1977).
[8]M. C. Lemaire and K. S. Low, Phys. Rev. C 16, 183 (1977).
[9]A. J. Baltz and S. Kahana, Phys. Rev. C 17, 555 (1978).
[10]D. K. Scott, B. G. Harvey, D. L. Hendrie, U. Jahrnke, L. Kraus, C. F. Maguire, J. Mahoney, Y. Terrien, K. Yagi, and N. K. Glendenning, Phys. Rev. Lett. 34, 895 (1975).
[11]B. Sorensen, Phys. Lett. 66B, 119 (1977).
[12]N. K. Glendenning and G. Wolshin, Phys. Rev. Lett. 34, 1642 (1975).
[13]K. Yagi, D. L. Hendrie, L. Kraus, C. F. Maguire, J. Mahoney, D. K. Scott, Y. Terrien, T. Udagawa, and T. Tamura, Phys. Rev. Lett. 34, 96 (1975).
[14]B. Saghai and P. Roussel, Nucl. Instrum. and Methods 141, 93 (1977).
[15]L. C. Northcliffe, Annu. Rev. Nucl. Sci. 13, 67 (1963).
[16]D. Brink, Phys. Lett. 40B, 37 (1972).
[17]F. Pougheon and P. Roussel, Phys. Rev. Lett. 30, 1223 (1973).
[18]R. Jahn, D. P. Stahel, G. J. Vozniak, R. J. De Meijer, and J. Cerny (unpublished).
[19]D. G. Kovar, in *Proceedings of the International Conference on Reactions Between Complex Nuclei, Nashville, Tennessee, 1974,* edited by R. L. Robinson, F. K. McGowan (North-Holland, Amsterdam, 1974), Vol. 2, p. 235.
[20]W. Henning, D. G. Kovar, B. Zeidman, and J. R. Erskine, Phys. Rev. Lett. 32, 1015 (1974).
[21]T. Tamura and K. S. Low, Comput. Phys. Commun. 8 (1974), SATURN-MARS I; T. Tamura, and K. S. Low, and T. Ugadawa, reports SATURN-MARS II (unpublished.
[22]T. Tamura, Phys. Rep. 14C, 59 (1974).
[23]T. A. Brody and M. Moshinsky, *Tables of Transformation Brackets for Nuclear Shell Model Calculations* (Gordon and Breach, New York, 1967).
[24]W. Chung, H. Nann, and B. Wildenthal (unpublished).
[25]K. Siwek-Wilczynska, J. Wilczyński, and P. R. Christensen, Nucl. Phys. A229, 461 (1974).
[26]J. R. Erskine, W. Henning, D. G. Kovar, L. R. Greenwood, and R. M. Devries, Phys. Rev. Lett. 34, 680 (1975).
[27]J. G. Cramer, R. H. Devries, D. A. Goldberg, M. S. Zisman, and C. F. Maguire, Phys. Rev. C 14, 2157 (1976).
[28]J. Raynal, Saclay Report No. D-Ph-T/69-42 (unpublished).
[29]M. E. Cobern, M. C. Lemaire, K. S. Low, M. C. Mermaz, H. Sztark, T. Udagawa, and T. Tamura, Phys. Rev. C 13, 1200 (1976).
[30]A. J. Baltz and S. Kahana, Phys. Rev. Lett. 29, 1267 (1972).
[31]B. F. Bayman, Phys. Rev. Lett. 32, 71 (1974).
[32]D. H. Feng, T. Ugadawa, and T. Tamura, Nucl. Phys. A274, 262 (1976).
[33]J. Raynal, Saclay Report No. D-Ph-T/72-78, 1971 (unpublished).
[34]P. H. Stelson and L. Grodzins, Nucl. Data 1, 1 (1965).
[35]A. H. Kleinfeld *et al.*, Phys. Rev. Lett. 35, 1329 (1975).
[36]R. M. Siemssen, Proceedings of the Symposium held at the ANL, Report No. ANL 7837 (unpublished).
[37]W. Mittig, P. Charles, S. H. Lee, I. Badawy, B. Berthier, B. Fernandez, and J. Gastebois, Nucl. Phys. A233, 48 (1974).
[38]T. R. Fisher, T. T. Bardin, J. A. Becker, L. F. Chase, Jr. D. Koller, R. E. McDonald, A. R. Poletti, and J. G. Pronko, Phys. Rev. C 7, 1878 (1973).